AD-A119 710 ALBERTA UNIV EDMONTON DEPT OF CHEMISTRY F/G 7/4
SIMULATION OF EDGE EFFECTS IN ELECTROANALYTICAL EXPERIMENTS BY --ETC(U)
AUG 82 B SPEISER, S PONS N00014-A2-G-0017
UNCLASSIFIED TR-14 NL

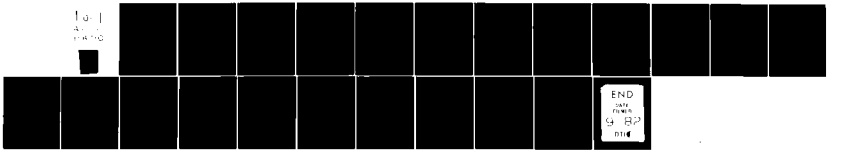

(12)

OFFICE OF NAVAL RESEARCH

Contract N00014-82-G-0017

Task No. NR 359-718

TECHNICAL REPORT NO. 14

Simulation of Edge Effects in Electroanalytical Experiments by Orthogonal Collocation. Part III. Application to Chronoamperometric Experiments.

By

Bernd Speiser and Stanley Pons

Prepared for Publication In

Electrochimica Acta

University of Alberta
Department of Chemistry
Edmonton, Alberta, Canada
T6G 2G2

August 18, 1982

SECURITY CLASSIFICATION OF THIS PAGE (When Data Entered)

REPORT DOCUMENTATION PAGE	READ INSTRUCTIONS BEFORE COMPLETING FORM
1. REPORT NUMBER: 14	2. GOVT ACCESSION NO: AD A118710	3. RECIPIENT'S CATALOG NUMBER
4. TITLE (and Subtitle): Simulation of Edge Effects in Electroanalytical Experiments. Part III. Application to Chronoamperometric Experiments.	5. TYPE OF REPORT & PERIOD COVERED: Technical Report # 14
	6. PERFORMING ORG. REPORT NUMBER
7. AUTHOR(s): Bernd Speiser and Stanley Pons	8. CONTRACT OR GRANT NUMBER(s): N00014-82-G-0017
9. PERFORMING ORGANIZATION NAME AND ADDRESS: Department of Chemistry, University of Alberta, Edmonton, Alberta, Canada T6G 2G2	10. PROGRAM ELEMENT, PROJECT, TASK AREA & WORK UNIT NUMBERS: Task No. NR 359-718
11. CONTROLLING OFFICE NAME AND ADDRESS: Office of Naval Research, Chemistry Program - Chemistry Code 472, Arlington, Virginia 22217	12. REPORT DATE: August 18, 1982
	13. NUMBER OF PAGES: 45
14. MONITORING AGENCY NAME & ADDRESS (if different from Controlling Office)	15. SECURITY CLASS. (of this report): Unclassified
	15a. DECLASSIFICATION/DOWNGRADING SCHEDULE
16. DISTRIBUTION STATEMENT (of this Report): This document has been approved for public release and sale; its distribution unlimited.	
17. DISTRIBUTION STATEMENT (of the abstract entered in Block 20, if different from Report)	
18. SUPPLEMENTARY NOTES	
19. KEY WORDS (Continue on reverse side if necessary and identify by block number): Electrochemistry, Chronoamperometry, Simulation, Orthogonal Collocation.	
20. ABSTRACT (Continue on reverse side if necessary and identify by block number): Comparisons of simulated results with theory for chronoamperometric systems is presented. Results for complicated systems are obtained with high accuracy in very short periods of time.	

DD FORM 1473 EDITION OF 1 NOV 65 IS OBSOLETE S/N 0102-LF-014-6601

Unclassified
SECURITY CLASSIFICATION OF THIS PAGE (When Data Entered)

SIMULATION OF EDGE EFFECTS IN ELECTROANALYTICAL EXPERIMENTS BY ORTHOGONAL COLLOCATION. PART 3*. APPLICATION TO CHRONOAMPEROMETRIC EXPERIMENTS

Bernd Speiser and Stanley Pons

Department of Chemistry
University of Alberta
Edmonton, Alberta, Canada
T6G 2G2

ABSTRACT

The theory of two-dimensional collocation has been employed to simulate a model describing chronoamperometric experiments under conditions where edge diffusion has to be taken into account. The influence of the dimensionless parameters, β and β', the initial integration stepwidth, $\Delta T'_0$, the number of collocation points, N, and the kind of polynomial used to approximate the real solution are investigated and discussed. An additional transformation of the radial coordinate is introduced. The numerical values for a large number of simulations with different sets of the above parameters are compared to reference values.

*Part 1; see ref. [1]

INTRODUCTION

In part 1 [1] of this series we derived the theory for the application of orthogonal collocation to the simulation of two-dimensional models. These are discribed by partial differential equations with two independent space variables and the time variable t. Let us consider a two-dimensional diffusion situation to a flat, circular electrode, where diffusion not only perpendicular to the surface may occur. This additional diffusion is called edge diffusion. The concentration c of each species is given by a partial differential equation of the form

$$\frac{\partial c}{\partial t} = D\left[\frac{\partial^2 c}{\partial x^2} + \frac{1}{r}\frac{\partial c}{\partial r} + \frac{\partial^2 c}{\partial r^2}\right] - f(c) \qquad (1)$$

where x is the distance perpendicular to the surface and r is the radial distance from the centre of the electrode. The "kinetic term" f(c) is determined by chemical reactions of the given species.

Our goal is to calculate c as a function of x and r at any time t under a set of initial and boundary conditions. The initial conditions model the experimental starting conditions, i.e. in general only the starting compound is present in a homogeneous solution. The boundary conditions specify the particulars of the experiment performed, e.g. chronoamperometry, cyclic voltammetry or another electroanalytical method.

Orthogonal collocation [2,3] approximates the real solution of partial differential equations, e.g. (1), by orthogonal polynomials, such that the differential equation is fulfilled at

certain points, the collocation points. This provides a method to reduce the partial differential equations to a system of coupled ordinary differential equations.

In part 1 of this series [1] we used a product of two polynomials in x and r respectively as approximation function to the real solution of our two-dimensional model for edge effects. We solved a system of 3 equations of type (1) describing an EC mechanism

$$A \overset{-ne^-}{\underset{+ne^-}{\rightleftharpoons}} B \qquad E^0,n \qquad (2)$$

$$B \overset{k}{\rightarrow} C \qquad (3)$$

under the boundary conditions valid for chronoamperometric experiments.

This second part of our series demonstrates the application of the derived theory to chronoamperometry. We examine the influence of several parameters on the numerical solutions of the simulations: the dimensionless parameters β and β', the integration stepwidth $\Delta T'_0$, the number of collocation points N, and the type of polynomial we are using to approximate the real solution. Also, we investigate the effect of choosing a different dimensionless coordinate system.

The calculations herein have been performed using only the concentration of the substrate A at the collocation points, because the current through the electrode may be calculated from the concentration profiles of A only. The concentration profiles

of species B and C, however, may be calculated from the formulae in part 1 [1].

We compare our numerical simulations to the results derived by an exact solution of a related problem by Oldham [4]. These numbers compare very well with solutions calculated by Aoki and Osteryoung [5] and Nakihana et al. [6], all using different approaches to compute values for the current at a finite disc electrode under chronoamperometric conditions with consideration of edge effects. All these approaches, however, are restricted to a very simple mechanism, the reversible electron transfer. The method of orthogonal collocation, however, is - once derived for a specific type of model, e.g. a two-dimensional model - very easily used to simulate all possible kinds of electrode mechanism. We only have to change the kinetic terms f(c) in our partial differential equations (1). Equations describing other species than A, B or C are very similar in form to those already derived [1]. This will be shown in part 3 of this series [7] for the boundary conditions of cyclic voltammetry. Also, changes in mechanisms require only minor changes of the computer code used to calculate numerical data. Thus, orthogonal collocation proves to be a flexible method to generate simulated values for electrochemical experiments modelled by two-dimensional diffusion equations.

THE DIMENSIONLESS PARAMETERS β AND β'

To perform the method of orthogonal collocation we have to normalize our problem into a space [0,1] in both directions x and

r. Also, we have to divide the r-space into an inner and an outer segment, simulated by two different functions. We denote the new distance coordinate perpendicular to the electrode as X, and refer to the normalized inner radial segment as R while using R' for the outer coordinates. The dimensionless simulation time is T'.

After substituting the transformation equations given in part 1 [1] we arrive at normalized differential equations which contain two dimensionless parameters, β and β':

$$\beta = \frac{r_0^2}{L^2} \tag{4}$$

$$\beta' = \frac{r_0^2}{(M-r_0)^2} \tag{5}$$

Here, r_0 is the radius of the electrode disc, imbedded in an insulator. The quantity L is a distance in X direction from the electrode at which no diffusion occurs during the simulated experiment, while M is an analogous distance in r-direction. Thus, L and M define a region in real space which is simulated in the calculations. The real points corresponding to our N collocation points are distributed within this space. We consider two limiting cases for L. An analogous discussion may be applied to M.

First, L may be very large. Then the points corresponding to the collocation points in real space, i.e. those points at which the concentration of the species involved is calculated, are spread over a large distance. The diffusion layer in which

the concentration of a species is depleted or increased, however, is very narrow in the beginning of the simulation. It increases with $t^{1/2}$. Thus, at short times, corresponding to small values of the dimensionless simulation time T', the diffusion may have *reached only few or none* of the points at which the concentration is calculated. Consequently, the numerical values calculated may not represent a good approximation to the real solution of our model and yield erroneous results.

On the other hand, if L is very large, we are looking at a very narrow layer of solution in real space. Even after a short time the diffusion layer may have reached all of our points and the boundary condition that no diffusion occurs at X = 1 (corresponding to x = L) is no longer true. We are using the mathematical formulation of this boundary condition [c_A^* (X=1) = 1] in our calculations and thus the numerical values may deviate from the real solution after this is happening.

We expect that the approximation solution given by orthogonal collocation is valid only in a certain time range and that this range depends on the values of β and β' chosen.

For all calculations referred to in this paper we used the condition β = β'. We simulate a square space adjacent to the insulator, because

$$\frac{\beta}{\beta'} = 1 = \frac{(R - r_0)^2}{L^2} \qquad (6)$$

or

$$L = (R - r_0) \qquad (7)$$

Figures 1a-c show calculated values for the current obtained including edge effects divided by the ideal Cottrell current. Comparing simulations using Legendre polynomials of degree N = 6 in both dimensions but different values for β = β' with the reference curve given by Oldham [4], we see that the above analysis is correct. For β = 1 good agreement over a wide range of the dimensionless simulation time is found ($2 \times 10^{-2} < T' < 1.1 \times 10^{-1}$). To give a specific example ($D = 1 \times 10^{-5}$ cm^2/s, r_0 = 0.1 cm), this range corresponds to real times t between 2×10^1 and 1.1×10^2 s according to the transformation equation relating t and T' [1]. At short times the error is considerable and it can be seen that the solution needs a number of integration steps to become stable. At longer times the collocation simulation result increases faster than Oldham's curve. This simulation needed 60 s cpu-time to calculate the entire curve ($10^{-4} < T' < 1.8 \times 10^{-2}$).

More accurate simulations for shorter times may be obtained using larger values for β. For example, with β = 10 in a range between $T' = 2 \times 10^{-3}$ and 1.2×10^{-2} good agreement with Oldham's curve is found, while β = 100 gives a reasonable approximation for $2 \times 10^{-4} < T' < 1.1 \times 10^{-3}$. In the latter cases significant deviation from Oldham's curve is seen at a time when our numerical values increase. This occurs at the same time as the calculated concentration at one of the outmost collocation point in the X-direction becomes smaller than about 0.98, thus confirming our conclusions drawn above. With increasing β,

however, the oscillating deviations at the beginning occur in a narrower time frame, again in accordance with our analysis.

The same behavior may be seen if we use polynomials with a larger number of collocation points (N = 9, 12,15; Figures 2-4). Now the "critical concentration" at the outmost collocation points moves nearer to unity, being about 0.996 for N = 9. The time T' at which the deviations occur, however, is almost the same as for N = 6. This leads to the empirical conclusion, that the upper time limit of the simulations is only determined by β. An analogous approch has been used by Whiting and Carr [2]. They defined the maximum simulation time which is accessible with a certain β as $T'_{max} < 0.15/\beta$. In our case we have the condition

$$T'_{max} < 0.1/\beta \qquad (8)$$

to be within the usable time range.

THE NUMBER OF COLLOCATION POINTS N

In the preceding paragraph we have seen that the number of collocation points N has a marked influence on the simulated numerical values. Thus, we compare curves obtained with different numbers N but using the same other parameters in Figure 5.

As N increases, the net of collocation points becomes more narrow, forcing the approximation function to fulfill the differential equation at more and more points exactly. This has

two effects: first, the overall solution becomes more accurate but we also have more simulation points near the boundaries (using Legendre polynomials, the collocation points are more densly spaced near X = 0 and X = 1 than around X = 0.5). Thus, for short times, we have more points to represent the steep concentration profile exhibited shortly after applying the potential pulse and we expect the range within which the oscillating deviations from the reference solution occur to be more narrow. With increasing N, the overall solutions should reach a common limiting value which should be a good approximation to the real solution.

Comparing the results given in Figure 5 we see that this is true. By increasing the number of collocation points from N = 6 to N = 15 the range in which no useful results are to be obtained because oscillations occur decreases by a factor of about 10, giving very good approximations from $2 * 10^{-3}$ - $3 * 10^{-2}$ dimensionless time units. The upper limit of the useful range is not affected, as Figures 1-4 show.

Also, the results differ only little (~ 0.4% when increasing N from 12 to 15) with increasing N. This shows the consistency of the calculations. The "limiting" values reached are very close to Oldham's solution [4].

Increasing the number of collocation points gives more and more accurate results as is to be expected. However, the cpu time used to perform the simulations in a given range also increases considerably. While integrating a system of 2 * 6 * 6 = 72 ordinary differential equations in the case of N =

6 we have to deal with 162, 288 and 450 such equations if we use 9, 12 or 15 interior collocation points, respectively. The average cpu time needed to calculate one concentration profile increases by a factor of 10 when N is increased from 6 to 15.

THE INTEGRATION STEPWIDTH

The next parameter we want to discuss is the initial integration stepwidth, $\Delta T'_o$. This is an input parameter for the subroutine performing the integrations of our system of ordinary differential equations. The value choosen is used by the subroutine to calculate the first concentration profiles at $\Delta T'_o$. The subroutine DHPCGL (in the SSP library package) used by us then "decides" if sufficient accuracy is available with this value. If not, the stepwidth is divided by 2 and the calculation is repeated. Other integration subroutines, e.g. STIFF3 [3], also have the option to increase the initial stepwidth if the error is below a specific margin.

To evaluate the influence of $\Delta T'_o$ on the accuracy and performance of the edge effect calculations we run simulations with N = 6 and 9 using $\Delta T'_o$ values ranging from 10^{-2} to 10^{-5}. Results for $\beta = \beta' = 1$ are given in Tables 1 and 2. We see immediately that the actual value of $\Delta T'_o$ has only a very small effect on the numerical simulation results. Deviations are 0.00007 in the worst case, this corresponds to 0.007%. However, for a small $\Delta T'_o$ (10^{-5} dimensionless time units), the cpu-time needed to simulate the model up to a certain time increases considerably. The savings using $\Delta T'_o$ values > 10^{-3} are only

about 10-20%. With large initial integration stepwidths there is not enough accuracy at the beginning of the simulation, thus causing DHPCGL to cut down $\Delta T'_o$ to smaller values. The actual choice of $\Delta T'_o$, however, seems not to be critical.

COMPLETE SIMULATIONS USING LEGENDRE POLYNOMIALS

After discussing three of the parameters used in simulations of chronoamperometric experiments with consideration of edge effects, we may now choose sets of parameters to obtain an approximate solution of the differential equations over a large range of the dimensionless simulation time. The number of interior collocation points will be 15. We will piece together the curve from solutions calculated with different β's, choosing the appropriate initial integration stepwidth. The trial functions will be Legendre polynomials.

The result is given in Figure 6, where the calculated current divided by the "ideal" Cottrell current is plotted against T' (in logarithmic scale). Four different values for β(1000, 100, 10, 1) have been used and the entire curve compares very well with Oldham's results [4]. The total cpu-time needed to calculate our curve was about 1340 s on an Amdahl 470/V6 computer. We cover, however, more than 4 orders of magnitude of the dimensionless simulation time. Using the same constants for D and r_0 as above, we simulated the response of an electrode with edge effects from 4 ms up to 30 s. At the lower limit ($T' \approx 2.5 \cdot 10^{-6}$) the current with edge effects deviates only by about 0.05% from the Cottrell current, while at the upper

limit ($T' \approx 3\times10^{-2}$) the current in real experiments may be affected by convection, thus giving rise to another kind of non-ideal behavior. Therefore, we can cover the entire accessible time range in which edge effects contribute to the experimental current with this simulation.

OTHER POLYNOMIALS

Orthogonal collocation may be performed using a variety of trial functions as long as we have a set of complete and linearly independent functions [8]. A certain class of sets fulfilling these conditions are the Jacobi polynomials $P_N^{(\delta,\varepsilon)}(x)$ given by [3]

$$P_N^{(\delta,\varepsilon)}(x) = \sum_{i=0}^{N} (-1)^{N-i} \gamma_i x^i, \quad \gamma_0 = 1 \tag{9}$$

with the orthogonality condition

$$\int_0^1 x^{\varepsilon}(1-x)^{\delta} P_j(x) P_{N(x)} = 0 \quad j = 0, 1\ldots, N-1 \tag{10}$$

The two terms x^{ε} and $(1-x)^{\delta}$ are "weight"factors" which determine the behavior of the function at the boundaries. For $\varepsilon \neq 0$ the function goes to zero at $x = 0$, for $\delta \neq 0$ zero is reached for $x = 1$. In our case the radial functions have nonzero values at both boundaries. Also, the x-functions in our outer space have a finite value at $x = 0$ (the insulator).

Thus, we would expect the best set of trial functions to be Legendre polynomials, $P_N^{(0,0)}(x)$ with $\delta = \varepsilon = 0$. We used Legendre

polynomials in all previous calculations in this paper, but tried also several other polynomials for the radial discretization function (e.g. $\delta = 0$, $\varepsilon = 2$ and $\delta = 1$, $\varepsilon = 0.5$ which yielded good results for problems with spherical symmetry).

The calculations showed that in all these cases the simulation results gave poorer agreement with Oldham's solution. We conclude therefore that the use of Jacobi type functions other than Legendre polynomials cannot be recommended in our case, due to the form of the boundary value problem.

ADDITIONAL TRANSFORMATION OF THE RADIAL VARIABLE R

After having simulated the concentration profile in our model we wish to calculate the current through the electrode as a function of time. In order to compare this current to the "ideal" Cottrell current we derived the expression (11) [1]:

$$\frac{it^{1/2}}{it^{1/2}_{\text{Cottrell}}} = 2\sqrt{\delta+T'} \int_0^1 R \left(\frac{\partial C^*_{Al}}{\partial X}\right)_{X=0} dR \tag{11}$$

where we have to integrate the product of R and the flux to the electrode surface over the entire radius of the circular electrode.

This integration may be performed by a quadrature formula

$$\int_0^1 y(r)\, w_k(r) dr = \sum_{l=1}^{N_r+2} Q_l\, Y_l \tag{12}$$

where the Q_l depend on the trial function used [1].

The form of the integral in equation (11) would suggest a

trial function with $\delta = 0$ and $\varepsilon = 1$. We have seen in the last paragraph, however, that the only suitable trial functions for our problem are Legendre polynomials with $\delta = \varepsilon = 0$. Thus, it is desirable to bring (11) into a form with $\delta = \varepsilon = 0$ by a variable transformation.

This may be done by the substitution

$$\Omega = R^2 \tag{13}$$

Then

$$dR = \frac{1}{2\Omega^{1/2}} d\Omega \tag{14}$$

and

$$dR^2 = \frac{1}{\Omega} d\Omega^2 \tag{15}$$

The integral in equation (11) reduces to

$$\frac{1}{2} \int_0^{1'} \left(\frac{\partial C_{A1}^*}{\partial X}\right)_{X=0} d\Omega \quad -$$

thus having a form consistent with $\delta = \varepsilon = 0$.

We have to apply transformations (13)-(15) to the differential equation describing the inner part of our model (see equation (26), part 1 of this series [1]) and to the boundary condition at $R = 1$ ($R' = 0$), where we piece together the inner and outer function (equation (50) in part 1 [1]).

The result for species A is

$$\frac{\partial c_{A1}^*}{\partial T'} = \beta \frac{\partial^2 c_{A1}^*}{\partial X^2} + 2 \frac{\partial c_{A1}^*}{\partial \Omega} + 4\Omega \frac{\partial^2 c_{A1}^*}{\partial \Omega^2} \tag{16}$$

and the boundary condition changes to

$$\left(\frac{\partial c_{A1}^*}{\partial \Omega}\right)_{\Omega=1} = \frac{\sqrt{\beta'}}{2} \left(\frac{\partial c_{A2}^*}{\partial R'}\right)_{R'=0} \tag{17}$$

If we substitute these equations for equations (26) and (50) in part 1 [1] and repeat the derivation of the discretized formulae (98) and (104) in part 1 [1] we find a new, very similar system of ordinary differential equations.

In fact, we only have to change the definition of the matrix elements $E_{l,k}$ to

$$E_{l,k} = 2.C_{l,k} + 4\Omega D_{l,k} \tag{18}$$

and substitute $\sqrt{\beta'/2}$ for $\sqrt{\beta'}$ in the definitions of the vector elements G_l, the matrix elements $L'_{l,k}$ and the discretized expression (98).

We calculated numerical values for this system. The results are given and compared to the nontransformed system in Figures 7-9 for N = 6, 9, 12. Values for N = 15 are compared in Table 3, while Figure 10 gives a curve pieced together using 4 calculations performed with N = 15 and different β values. The

numerical values are consistent with changes < 0.2% with N increasing by 3 in a region, where the oscillatory behavior at the beginning has stopped. Comparing to the nontransformed system and to Oldham's reference values, we find that the new equations give better values for a given number of collocation points. For N = 15 deviation from the reference values is in the range of 0.16% (Table 3).

Figure 10 also shows how well our numerical values compare to Oldham's model over more than 4 orders of magnitude in T'. While the nontransformed equations gave rise to a curve which was lower than Oldham's at shorter times and higher at longer times (Figure 6), we see that our transformed system gives values which are slightly lower than the reference over the entire range.

This example clearly shows that the choice of trial functions and transformations has an influence on the exact numerical solutions calculated. Good approximations, however, may be available with the "standard" method also (i.e. without consideration of the type of functions used). A more detailed investigation on the effect of using different sets of trial functions is currently under way.

CONCLUSIONS

Our two-dimensional diffusion model using orthogonal collocation has proved to provide good approximations for the current expected at a flat, circular electrode imbedded into an insulator over several orders of magnitude for the dimensionless time variable T'. The discussion of parameters in this paper

shows that even with only 6 interior collocation points, i.e. a grid of 2 × 6 × 6 = 72 collocation points in the entire simulation space, reliable numerical values may be obtained. With increasing number of collocation points the simulations are consistent and give even better approximations. However, longer cpu-times and costs to perform the calculations are necessary. We again like to point out that changes to different mechanisms requires only the exchange or addition of a few statements in the computer code. Thus, orthogonal collocation may be recommended as a fast and powerful method to simulate edge effects at electrodes.

REFERENCES

1. part 1: B. Speiser and S. Pons, Can. J. Chem. in press.
2. L.P. Whiting and P.W. Carr, J. Electroanal. Chem. 81, 1 (1977).
3. J. Villadsen and M.L. Michelson, Solution of Differential Equation Models by Polynomial Approximation, Prentice Hall, Englewood Cliffs, 1978.
4. K.B. Oldham, J. Electroanal. Chem. 122, 1 (1981).
5. K. Aoki and J. Osteryoung, J. Electroanal. Chem. 122, 19 (1981).
6. M. Kakihana, H. Ikeuchi, G.P. Sato and K. Tokuda, J. Electroanal. Chem. 108, 381 (1980).
7. B. Speiser and S. Pons, Can. J. Chem., submitted.
8. B.A. Finlayson in R. Bellman (Ed.) "Mathematics in Science and Engineering", Vol. 87, Academic Press, New York and London, 1972, p. 34

Table 1. Numerical values for simulation of a chronoamperometric experiment with edge effects: current with edge effects divided by Cottrell current simulation parameters: $N = 6$, $\beta = \beta' = 1$, [illegible] polynomials in both dimensions, $\Delta T'_o$ as indicated

$T'/\Delta T'_o$	10^{-2}	10^{-3}		10^{-5}
0.01	1.13249*	1.13256		1.13256
0.02	1.23881*	1.23884		1.23886
0.03	1.29817*	1.29816*	1	1.29817
0.04	1.34786*	1.34787*	1.34787	--
0.05	1.39292*	1.39292	1.39292	--
0.06	1.43443*	1.43444	1.43444	--
0.07	1.47305	1.47303*	1.47305	--
0.08	1.50926	1.50926	1.50926	--
0.09	1.54348	1.54350*	1.54349	--
0.1	1.57606	1.57607	1.57607	--

* Values calculated by interpolation.

Table 2. Numerical values for simulation of a chronoamperometric experiment with edge effects: current with edge effects divided by Cottrell current; simulation parameters: $N = 9$, $\beta = \beta' = 1$, Legendre polynomials in both dimensions, $\Delta T'_o$ as indicated.

$T'/\Delta T'_o$	10^{-2}	10^{-3}	10^{-4}	10^{-5}
0.01	1.17081*	1.17080	1.17082	1.17082
0.02	1.24847*	1.24848*	1.24848	--
0.03	1.30911	1.30911*	1.30911	--
0.04	1.36075	1.36075*	1.36076	--
0.05	1.40674	1.40672	1.40673	--
0.06	1.44862*	1.44864	1.44864	--
0.07	1.48748	1.48748*	1.48748	--
0.08	1.52387	1.52387	1.52387	--
0.09	1.55826*	1.55826	1.55826	--
0.1	1.59100	1.59100*	1.59100	--

* Values calculated by interpolation.

Table 3. Numerical values for simulation of a chronoamperometric experiment with edge effects: current with edge effects devided by Cottrell current; transformed simulation model vs nontransformed system, $N = 15$, $\beta = \beta' = 10$, Legendre polynomials in both dimensions.

T'	Oldham's solution [4]	transformed model	nontransformed model
1.10^{-4}	1.0175	1.0206	1.0192
2	1.0249	1.0221	1.0210
3	1.0305	1.0291	1.0278
4	1.0353	1.0338	1.0326
5	1.0395	1.0380	1.0367
6	1.0433	1.0416	1.0405
7	1.0468	1.0452	1.0441
8	1.0500	1.0485	1.0473
9	1.0531	1.0515	1.0504
1.10^{-3}	1.0560	1.0544	1.0534
2	1.0792	1.0776	1.0770
3	1.0970	1.0954	1.0953

FIGURE CAPTIONS

Figure 1. Simulations of chronoamperometric experiments including edge effects with orthogonal collocation; simulation parameters: number of collocation points in each dimension N = 6, initial integration stepwidth $\Delta T'_0 = 1.10^{-4}$, Legendre polynomials in both dimensions, (——) $\beta = 100$, (—·—·—) $\beta = 10$, (----) $\beta = 1$; (....) values calculated according to Oldham [4]. The arrows indicate T', when the concentration at one of the outmost collocation points reaches 0.98.

Figure 2. Simulations of chronoamperometric experiments including edge effects with orthogonal collocation; simulation parameters: number of collocation points in each dimension N = 9, other parameters as in Figure 1. The arrow indicates T', when the concentration at one of the outmost collocation points reaches 0.996.

Figure 3. Simulations of chronoamperometric experiments including edge effects with orthogonal collocation; simulation parameters: number of collocation points in each dimension N = 12, other parameters as in Figure 1.

Figure 4. Simulations of chronoamperometric experiments including edge effects with orthogonal collocation; simulation parameters: number of collocation points in each dimension N = 15, other parameters as in Figure 1. The ordinate scale is expanded compared to the other figures.

Figure 5. Simulations of chronoamperometric experiments including edge effects with orthogonal collocation; simulation parameters: (——) N = 6, (—·—·—) N=9, (----) N = 12, (—·—·—·—) N = 15; initial integration stepwidth $\Delta T'_0 = 1.10^{-4}$, Legendre polynomials in both dimensions, dimensionless parameters $\beta = \beta' = 1$, (....) values calculated according to Oldham [4].

Figure 6. Simulations to cover the entire accessible range of t for an example with $D = 10^{-5}$ cm^2/s and $r_0 = 0.1$ cm, pieced together from 4 calculations with N = 15 and different β compared to Oldham's solution (●●●); points calculated with $\beta = \beta' = 1000$ (■■■), $\beta = \beta' = 100$ (▲▲▲), $\beta = \beta' = 10$ (□□□), $\beta = \beta' = 1$ (◆◆◆).

Figure 7. Comparison of simulations using the model system given in part 1 of this series [1] and the formulae derived from the transformation (13); N = 6, $\beta = \beta' = 10$; (——) before transformation, (—·—·—) after transformation, (....) Oldham's curve.

Figure 8. Comparison of simulations using the model system given in part 1 of this series [1] and the formulae derived from the transformation (13); N = 9, $\beta = \beta' = 10$; (——) before transformation, (—·—·—) after transformation, (....) Oldham's curve.

Figure 9. Comparison of simulations using the model system given in part 1 of this series [1] and the formulae derived from the transformation (13); N = 12, $\beta = \beta' = 10$; (——) before transformation, (– – –) after transformation, (....) Oldham's curve.

Figure 10. Simulations to cover the entire time range $2.10^{-6} < T' < 4.10^{-2}$, pieced together from 4 calculations with N = 15 and different β, using the transformed system of equations, compared to Oldham's solution (●●●); points calculated with $\beta = \beta' \geq 1000$ (■■■), $\beta = \beta' = 100$ (⊙⊙⊙), $\beta = \beta' = 10$ (□□□) and $\beta = \beta' = 1$ (▲▲▲).

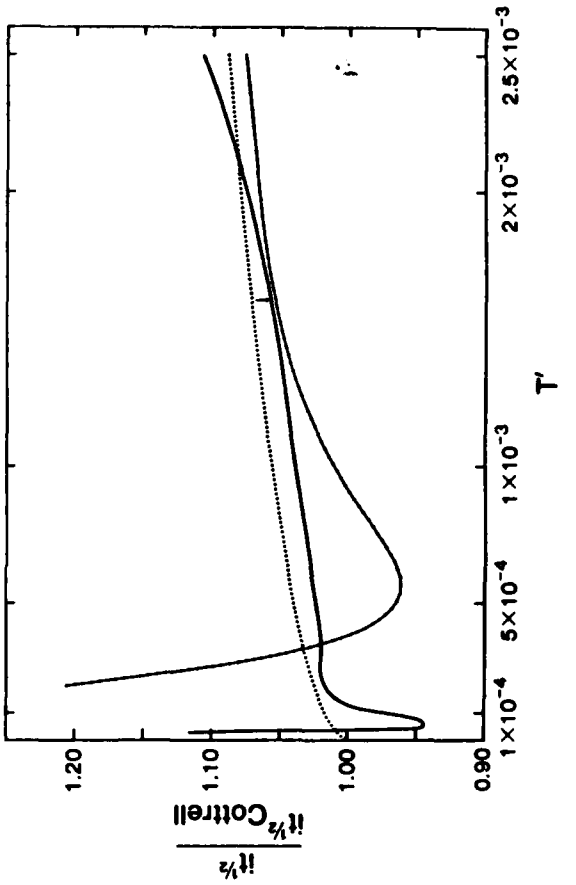

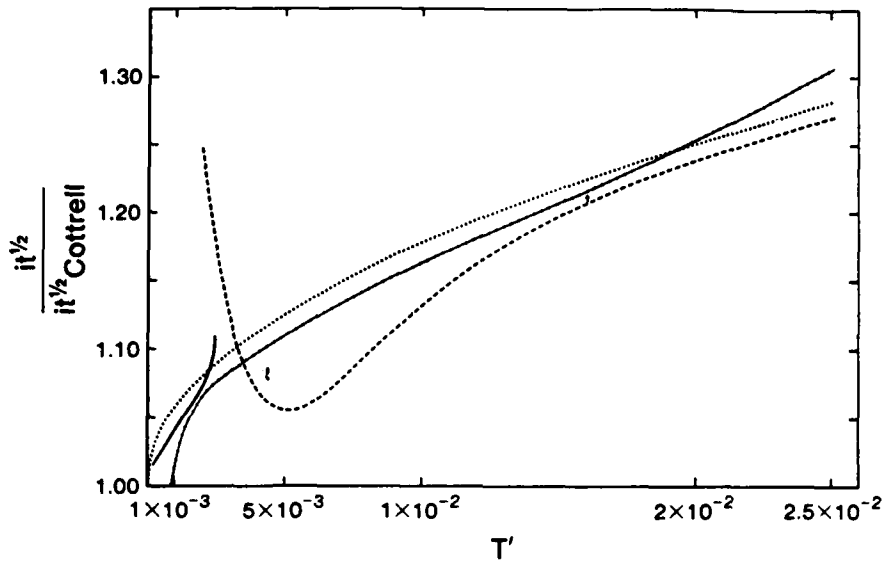
1.30
1.20
1.10
1.00
$\frac{it^{1/2}}{it^{1/2}_{Cottrell}}$
1×10^{-3}
5×10^{-3}
1×10^{-2}
2×10^{-2}
2.5×10^{-2}
T'

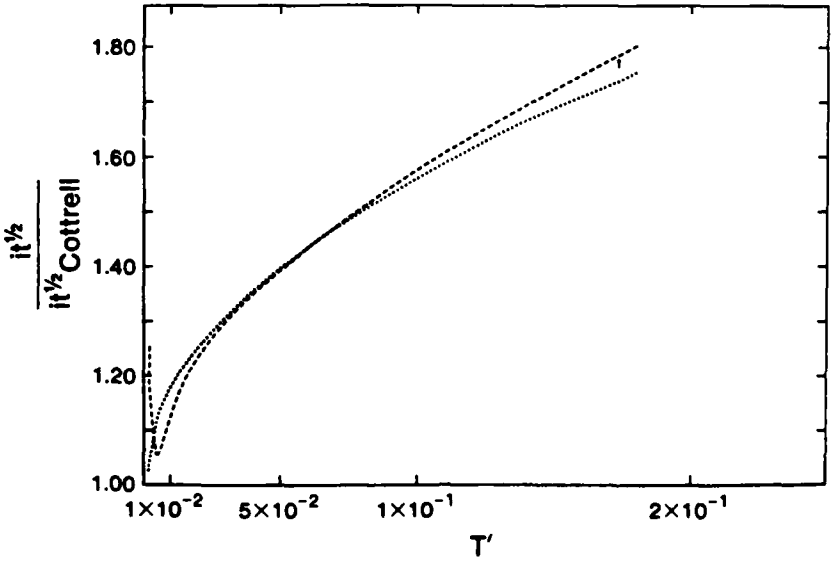
1.80
1.60
1.40
1.20
1.00
$\frac{it^{1/2}}{it^{1/2}_{Cottrell}}$
1×10^{-2}
5×10^{-2}
1×10^{-1}
2×10^{-1}
T'

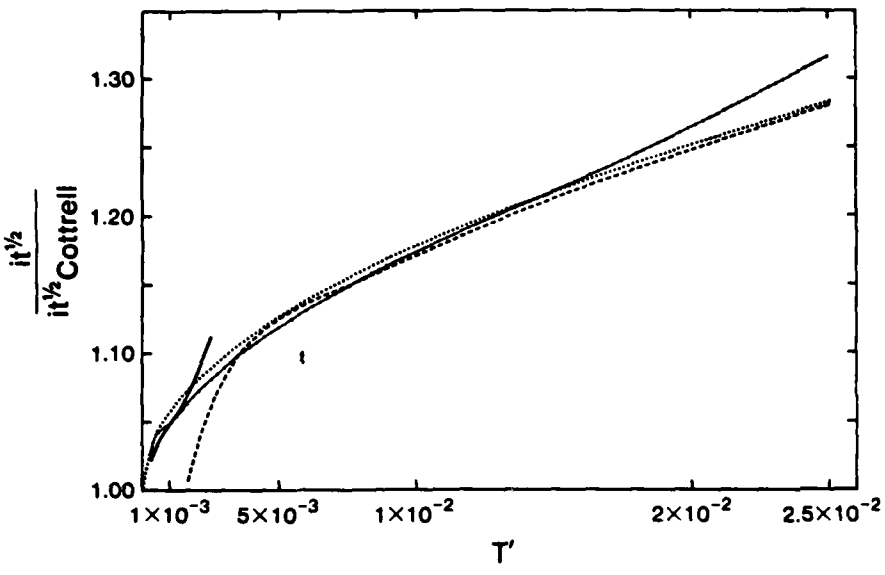
1.30
1.20
1.10
1.00
$\frac{it^{1/2}}{it^{1/2}_{Cottrell}}$
1×10⁻³
5×10⁻³
1×10⁻²
2×10⁻²
2.5×10⁻²
T′

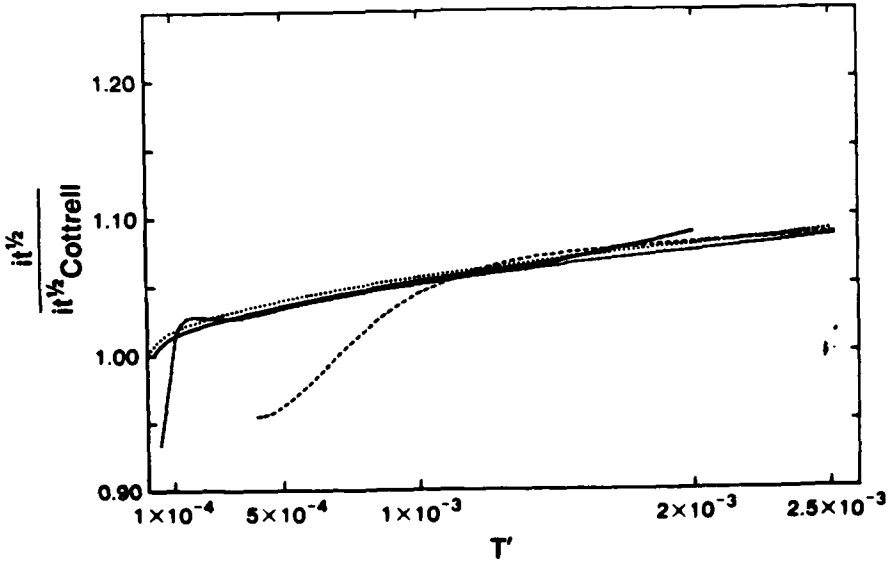
1.20
1.10
1.00
0.90
$\frac{it^{1/2}}{it^{1/2}_{Cottrell}}$
1×10⁻⁴
5×10⁻⁴
1×10⁻³
2×10⁻³
2.5×10⁻³
T′

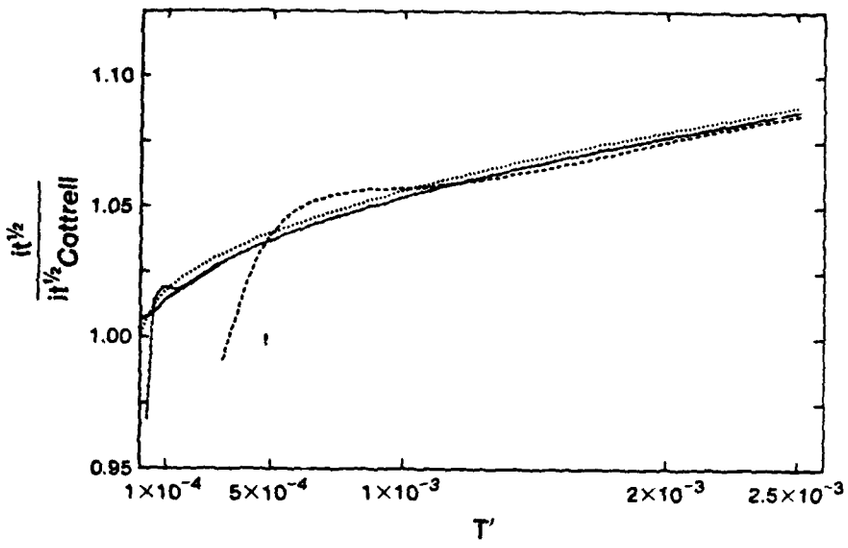
1.10
1.05
1.00
0.95
$\frac{it^{1/2}}{it^{1/2}Cottrell}$
1×10⁻⁴
5×10⁻⁴
1×10⁻³
2×10⁻³
2.5×10⁻³
T'

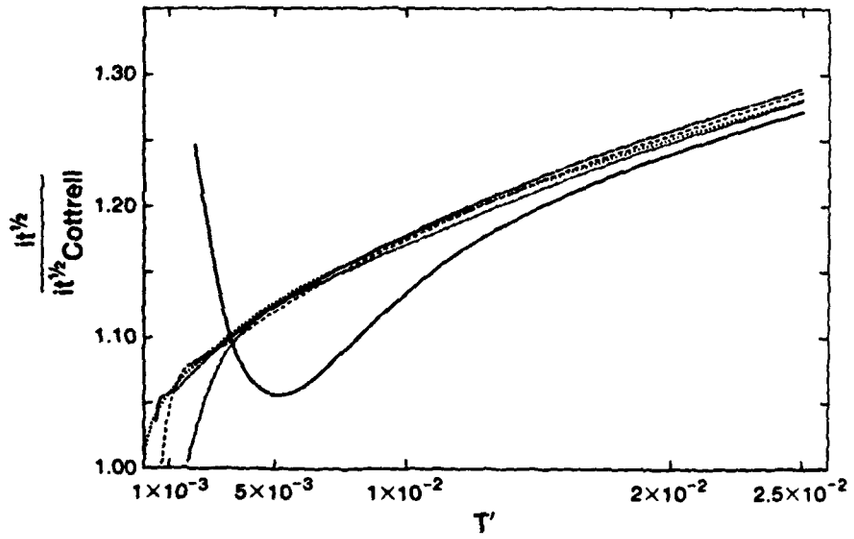
1.30
1.20
1.10
1.00
$\frac{it^{1/2}}{it^{1/2}Cottrell}$
1×10⁻³
5×10⁻³
1×10⁻²
2×10⁻²
2.5×10⁻²
T'

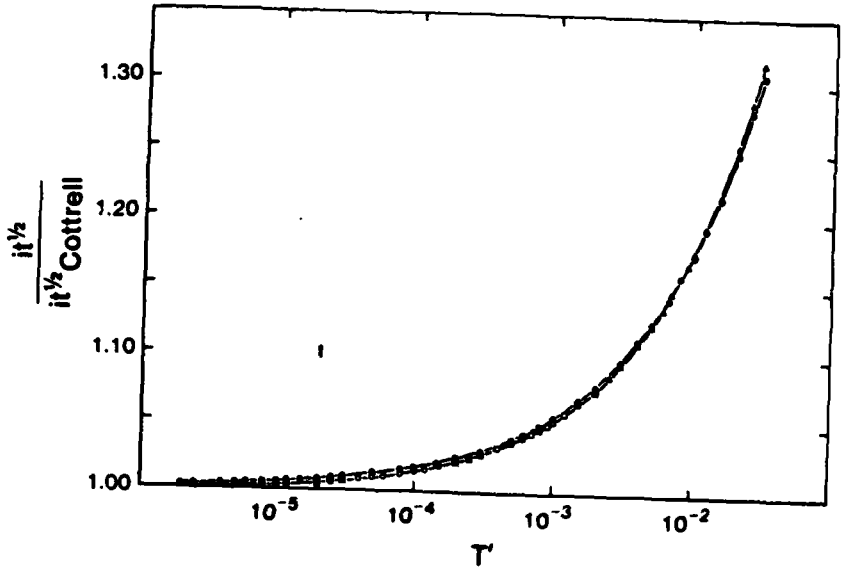
1.30
1.20
1.10
1.00
$\frac{it^{1/2}}{it^{1/2}_{Cottrell}}$
10^{-5}
10^{-4}
10^{-3}
10^{-2}
T'

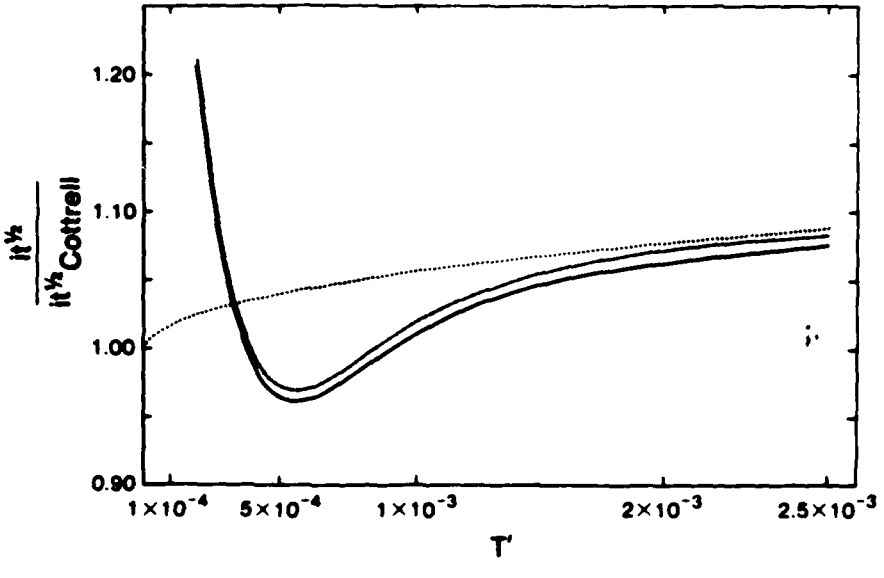
1.20
1.10
1.00
0.90
$\frac{it^{1/2}}{it^{1/2}_{Cottrell}}$
1×10^{-4}
5×10^{-4}
1×10^{-3}
2×10^{-3}
2.5×10^{-3}
T'

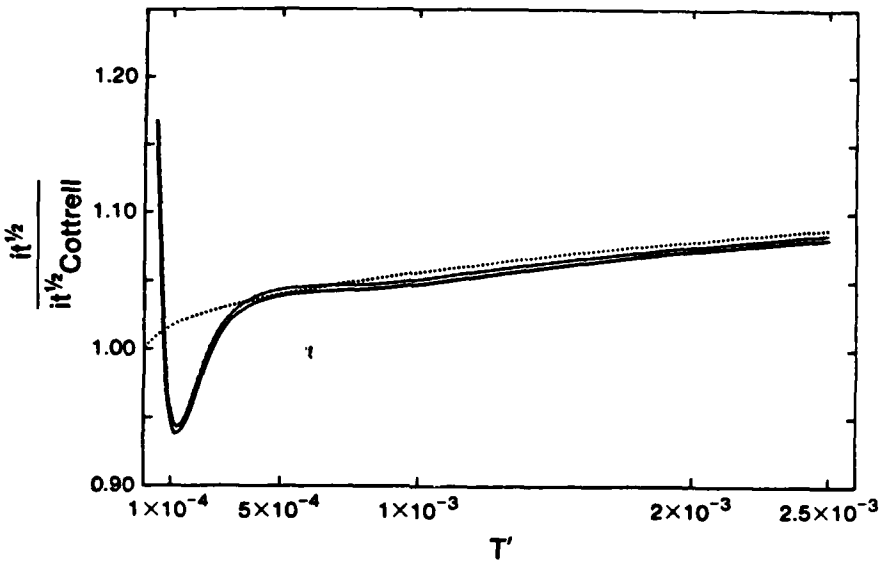
1.20
1.10
1.00
0.90
$\frac{it^{1/2}}{it^{1/2}_{Cottrell}}$
1×10⁻⁴
5×10⁻⁴
1×10⁻³
2×10⁻³
2.5×10⁻³
T'

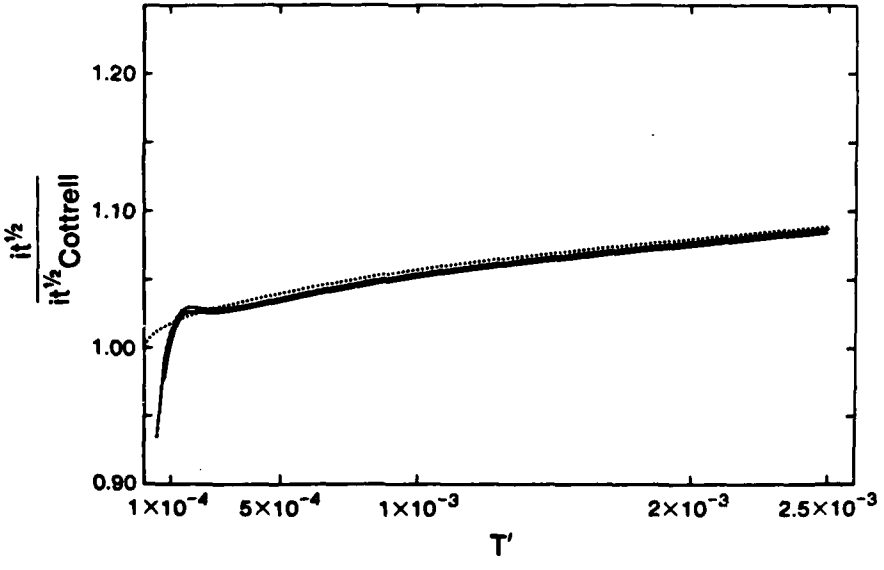
1.20
1.10
1.00
0.90
$\frac{it^{1/2}}{it^{1/2}_{Cottrell}}$
1×10⁻⁴
5×10⁻⁴
1×10⁻³
2×10⁻³
2.5×10⁻³
T'

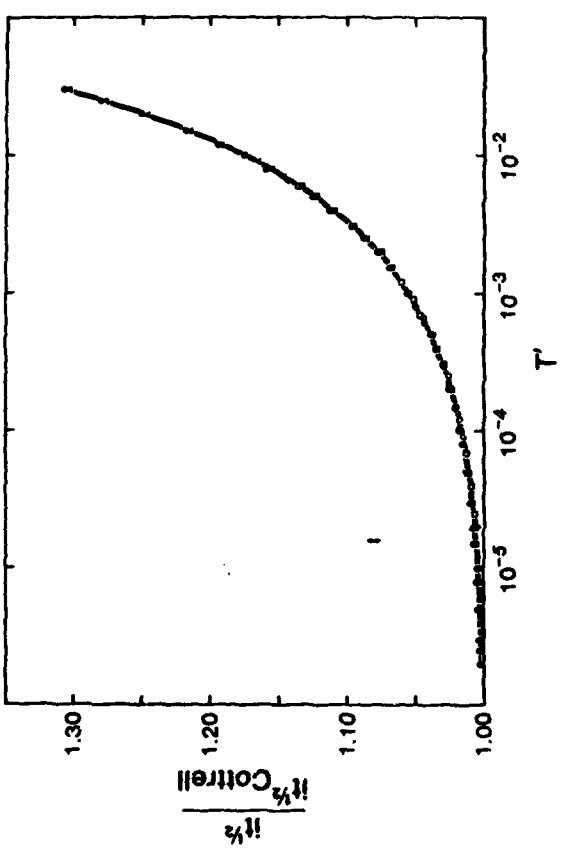

TECHNICAL REPORT DISTRIBUTION LIST, GEN

	No. Copies
Office of Naval Research Attn: Code 472 800 North Quincy Street Arlington, Virginia 22217	2
ONR Western Regional Office Attn: Dr. R. J. Marcus 1030 East Green Street Pasadena, California 91106	1
ONR Eastern Regional Office Attn: Dr. L. H. Peebles Building 114, Section D 666 Summer Street Boston, Massachusetts 02210	1
Director, Naval Research Laboratory Attn: Code 6100 Washington, D.C. 20390	1
The Assistant Secretary of the Navy (RE&S) Department of the Navy Room 4E736, Pentagon Washington, D.C. 20350	1
Commander, Naval Air Systems Command Attn: Code 310C (H. Rosenwasser) Department of the Navy Washington, D.C. 20360	1
Defense Technical Information Center Building 5, Cameron Station Alexandria, Virginia 22314	12
Dr. Fred Saalfeld Chemistry Division, Code 6100 Naval Research Laboratory Washington, D.C. 20375	1
U.S. Army Research Office Attn: CRD-AA-IP P.O. Box 1211 Research Triangle Park, N.C. 27709	1
Naval Ocean Systems Center Attn: Mr. Joe McCartney San Diego, California 92152	1
Naval Weapons Center Attn: Dr. A. B. Amster, Chemistry Division China Lake, California 93555	1
Naval Civil Engineering Laboratory Attn: Dr. R. W. Drisko Port Hueneme, California 93401	1
Department of Physics & Chemistry Naval Postgraduate School Monterey, California 93940	1
Scientific Advisor Commandant of the Marine Corps (Code RD-1) Washington, D.C. 20380	1
Naval Ship Research and Development Center Attn: Dr. G. Bosmajian, Applied Chemistry Division Annapolis, Maryland 21401	1
Naval Ocean Systems Center Attn: Dr. S. Yamamoto, Marine Sciences Division San Diego, California 91232	1
Mr. John Boyle Materials Branch Naval Ship Engineering Center Philadelphia, Pennsylvania 19112	1

TECHNICAL REPORT DISTRIBUTION LIST, 359

	No. Copies
Dr. Paul Delahay Department of Chemistry New York University New York, New York 10003	1
Dr. E. Yeager Department of Chemistry Case Western Reserve University Cleveland, Ohio 41106	1
Dr. D. H. Bennion Department of Chemical Engineering Brigham Young University Provo, Utah 84602	1
Dr. R. A. Marcus Department of Chemistry California Institute of Technology Pasadena, California 91125	1
Dr. J. J. Auborn Bell Laboratories Murray Hill, New Jersey 07974	1
Dr. Adam Heller Bell Laboratories Murray Hill, New Jersey 07974	1
Dr. T. Katan Lockheed Missiles & Space Co, Inc. P.O. Box 504 Sunnyvale, California 94088	1
Dr. Joseph Singer, Code 302-1 NASA-Lewis 21000 Brookpark Road Cleveland, Ohio 44135	1
Dr. B. Brummer EIC Incorporated 55 Chapel Street Newton, Massachusetts 02158	1
Library P. R. Mallory and Company, Inc. Northwest Industrial Park Burlington, Massachusetts 01803	1
Dr. P. J. Bendra Department of Chemistry University of Southhampton Southhampton SO9 5NH United Kingdom	1
Dr. Sam Perone Department of Chemistry Purdue University West Lafayette, Indiana 47907	1
Dr. Royce W. Murray Department of Chemistry University of North Carolina Chapel Hill, North Carolina 27514	1
Naval Ocean Systems Center Attn: Technical Library San Diego, California 92152	1
Dr. C. E. Mueller The Electrochemistry Branch Materials Division, Research & Technology Department Naval Surface Weapons Center White Oak Laboratory Silver Spring, Maryland 20910	1
Dr. G. Goodman Globe-Union Incorporated 5757 North Green Bay Avenue Milwaukee, Wisconsin 53201	1
Dr. J. Boechler Electrochimica Corporation Attention: Technical Library 2485 Charleston Road Mountain View, California 94040	1
Dr. F. P. Schmidt Department of Chemistry Oakland University Rochester, Michigan 48063	1
Dr. H. Richtol Chemistry Department Rensselaer Polytechnic Institute Troy, New York 12181	1

TECHNICAL REPORT DISTRIBUTION LIST, 359

	No. Copies
Dr. A. B. Ellis Chemistry Department University of Wisconsin Madison, Wisconsin 53706	1
Dr. M. Wrighton Chemistry Department Massachusetts Institute of Technology Cambridge, Massachusetts 02139	1
Larry E. Plew Naval Weapons Support Center Code 30736, Building 2906 Crane, Indiana 47522	1
S. Ruby DOE (STOR) 600 E Street Washington, D.C. 20545	1
Dr. Aaron Wold Brown University Department of Chemistry Providence, Rhode Island 02192	1
Dr. R. C. Chudacek McGraw-Edison Company Edison Battery Division Post Office Box 28 Bloomfield, New Jersey 07003	1
Dr. A. J. Bard University of Texas Department of Chemistry Austin, Texas 78712	1
Dr. M. M. Nicholson Electronics Research Center Rockwell International 3370 Miraloma Avenue Anaheim, California	1
Dr. Donald W. Ernst Naval Surface Weapons Center Code R-33 White Oak Laboratory Silver Spring, Maryland 20910	1
Dr. R. P. Van Duyne Department of Chemistry Northwestern University Evanston, Illinois 60201	1
Dr. R. Stanley Yoss Department of Chemistry University of Alberta Edmonton, Alberta CANADA T6G 2G2	1
Dr. Michael J. Weaver Department of Chemistry Michigan State University East Lansing, Michigan 48824	1
Dr. R. David Rauh EIC Corporation 55 Chapel Street Newton, Massachusetts 02158	1
Dr. J. David Margerum Research Laboratories Division Hughes Aircraft Company 3011 Malibu Canyon Road Malibu, California 90265	1
Dr. Harris Fleischmann Department of Chemistry University of Southampton Southampton SO9 5NH England	1
Dr. Janet Osteryoung Department of Chemistry State University of New York at Buffalo Buffalo, New York 14214	1
Dr. R. A. Osteryoung Department of Chemistry State University of New York at Buffalo Buffalo, New York 14214	1
Mr. James R. Haden Naval Underwater Systems Center Code 3632 Newport, Rhode Island 02840	1

TECHNICAL REPORT DISTRIBUTION LIST, 359

	No. Copies
Dr. R. Nowak Naval Research Laboratory Code 6130 Washington, D.C. 20375	1
Dr. John P. Houlihan Shenango Valley Campus Pennsylvania State University Sharon, Pennsylvania 16146	1
Dr. D. F. Shriver Department of Chemistry Northwestern University Evanston, Illinois 60201	1
Dr. D. H. Whitmore Department of Materials Science Northwestern University Evanston, Illinois 60201	1
Dr. Alan Bewick Department of Chemistry The University Southampton, S09 5NH England	1
Dr. A. Himy NAVSEA-5433 NC #4 2541 Jefferson Davis Highway Arlington, Virginia 20362	1
Dr. John Kincaid Department of the Navy Strategic System Project Office Room 901 Washington, DC 20376	1
N. L. Robertson Manager, Electrochemical Power Sonices Division Naval Weapons Support Center Crane, Indiana 47522	1
Dr. Elton Cairns Energy & Environment Division Lawrence Berkeley Laboratory University of California Berkeley, California 94720	1

	No. Copies
Dr. Bernard Spielvogel U.S. Army Research Office P.O. Box 12211 Research Triangle Park, NC 27709	1
Dr. Denton Elliott Air Force Office of Scientific Research Bolling AFB Washington, DC 20332	1
Dr. David Aikens Chemistry Department Rensselaer Polytechnic Institute Troy, NY 12181	1
Dr. A. P. B. Lever Chemistry Department York University Downsview, Ontario M3J1P3 Canada	1
Mr. Maurice P. Murphy Naval Sea Systems Command 63R32 2221 Jefferson Davis Highway Arlington, VA 20360	1
Dr. Stanislaw Szpak Naval Ocean Systems Center Code 6343 San Diego, CA 95152	1
Dr. Gregory Farrington Department of Materials Science & Engineering University of Pennsylvania Philadelphia, PA 19104	1
Dr. Bruce Dunn Department of Engineering & Applied Science University of California Los Angeles, CA 90024	1

TECHNICAL REPORT DISTRIBUTION LIST, 359

	No. Copies
Dr. Micha Tomkiewicz Department of Physics Brooklyn College Brooklyn, NY 11210	1
Dr. Lesser Blum Department of Physics University of Puerto Rico Rio Piedras, PR 00931	1
Dr. Joseph Gordon II IBM Corporation F33/281 5600 Cottle Road San Jose, CA 95193	1
Dr. Robert Somoano Jet Propulsion Laboratory California Institute of Technology Pasadena, CA 91103	1

END

DATE
FILMED

9 82

DTIC